Available online at www.sciencedirect.com
SCIENCE DIRECT®
EPSL
Earth and Planetary Science Letters 216 (2003) 27–41
www.elsevier.com/locate/epsl

Strength asperities along oceanic transform faults: a model for the origin of extensional earthquakes on the Eltanin transform system

Erin K. Beutel [a], Emile A. Okal [b,*]

[a] *Department of Geology, College of Charleston, Charleston, SC 29424, USA*
[b] *Department of Geological Sciences, Northwestern University, Evanston, IL 60208, USA*

Received 12 March 2003; received in revised form 5 August 2003; accepted 18 August 2003

Abstract

We use finite element simulations of the state of stress in the vicinity of the Eltanin transform system to investigate the possible origin of earthquakes occurring on, or in the immediate vicinity of, transform segments, and featuring normal faulting mechanisms with tension axes oriented approximately 45° away from the azimuth of plate motion, in principle unexpected along transform faults. In addition to solutions previously described in the literature, we report on seven new such mechanisms, including a large event with magnitude >6 in 2001. We model the transform segments as either weak, i.e., featuring the same elastic properties as the ridge, or strong, i.e., featuring the same properties as the surrounding cooled oceanic lithosphere. In addition, we allow irregularities in the geometry of the transform contact, in the form of either bends in the plate boundary ('jogs') or asperities, i.e., strong elements in an otherwise weak transform system. We also consider the effect of oblique ridge push on the Pacific plate. We conclude that the seismic properties of the Eltanin transform system are best described by the model of a weak transform, in which a few strong asperities are embedded. We speculate that their origin may be linked to the complex and recent history of readjustments in rates and directions of spreading, notably to the south of the Eltanin system.

Keywords: oceanic transforms; asperities; anomalous earthquakes; Eltanin Transform Fault

1. Introduction and background

The Eltanin transform system forms a major offset in the boundary between the Pacific and Antarctic plates, along the southern portion of the East Pacific Rise. As detailed on Fig. 1, it is composed of two major units, the Heezen and Tharp transform faults (TFs), separated by a 55-km-long ridge segment [1]. The Heezen TF is 380 km and the Tharp TF 480 km long; each is about 10 km wide at the rim and 6 km deep. SEABEAM mapping of the Heezen TF has shown a fault-bounded rift with anastamosing and en-échelon faulting in the valley floor, where it is believed that most of the motion is taken up. While detailed mapping of the Tharp TF is not

* Corresponding author. Tel.: +1-847-491-3194; Fax: +1-847-491-8060.
E-mail addresses: bentele@cofc.edu (E.K. Beutel), emile@earth.nwu.edu (E.A. Okal).

0012-821X/03/$ – see front matter © 2003 Elsevier B.V. All rights reserved.
doi:10.1016/S0012-821X(03)00484-9

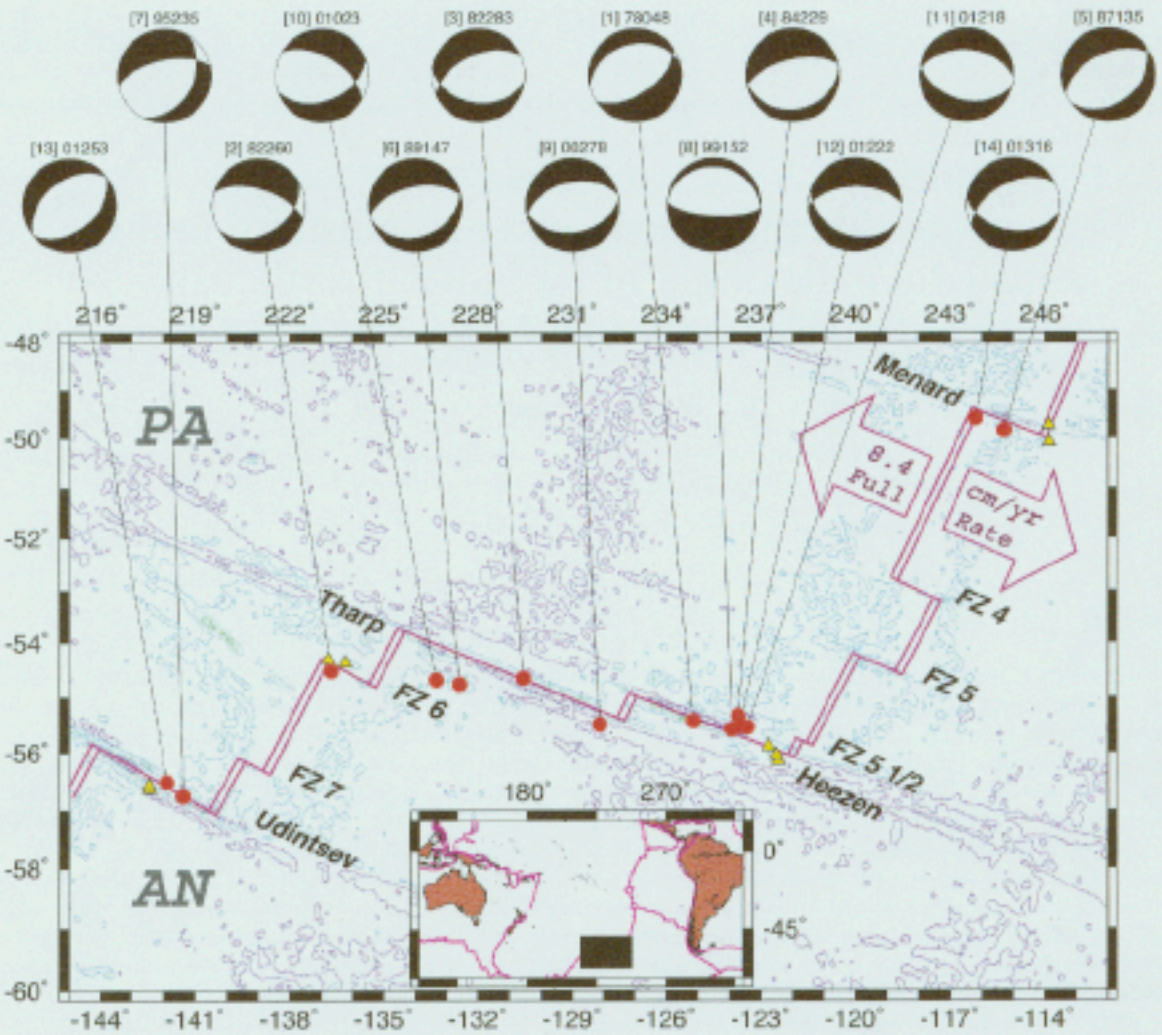

Fig. 1. Map of the Eltanin transform system in the South Pacific. The boundary between the Pacific (PA) and Antarctic (AN) plates, and their relative motion, are shown in purple (the full rate corresponds to a location on the Eltanin system). The principal FZs are labeled in black. The anomalous earthquakes listed in Table 1 are shown as red dots; each focal solution is shown as a beach ball and identified through index number (in brackets) and julian date (yyddd). The nine largest strike-slip solutions in the CMT Harvard catalog are shown as open triangles. The inset locates the main map (black square) inside the Pacific Basin.

yet available, it is believed that it is a twin of the Heezen TF, based on the rough geomorphology gleaned from gravity and satellite altimetry [1]. As determined by DeMets et al. [2], slip rates along the Eltanin system are between 80 and 84 mm/yr, at an azimuth of relative motion of N117°E.

Early seismological investigations of the Eltanin TF system [3] revealed a systematic deficiency of more than 90% in moment release as compared to kinematic models. More recently, Okal and Langenhorst [4] confirmed this deficiency using an improved, digital data set. They further relocated 75 yr of historical and modern seismicity, using the methodology pioneered by Wysession et al. [5], which includes a Monte Carlo algorithm injecting Gaussian noise into the data. They con-

cluded that earthquakes in the Eltanin region are generally confined to narrow lines of activity along well-defined transform segments. They found no areas of diffuse seismicity and the few identified outliers were located along supposedly inactive segments of the fracture zones (FZs) (e.g., the Heezen FZ and the so-called FZ $5\frac{1}{2}$).

Another intriguing property of the Eltanin TF system, described by Wolfe et al. [6], is the presence of anomalous, normal faulting earthquake mechanisms, expressing extension across the system. These results were confirmed and updated by Okal and Langenhorst [4], who documented a total of seven such events: two each on the Tharp and Heezen TFs, one on the Hollister TF immediately to the southwest, one on the Udintsev TF to the south, and one on the Menard TF to the north. Since their study was published, no fewer than seven additional normal faulting solutions have been documented on the Eltanin system and its adjoining TFs [7]. Table 1 lists the combined 14-event data set, which is also plotted on Fig. 1. The epicenters retained are from Engdahl et al. [8]; and from E.R. Engdahl (personal communication, 2002) for events predating 2000, from the ISC Bulletin from 2000 to January 2001, and from the USGS PDE thereafter. In this respect, the data set is inhomogeneous, but a case-by-case inspection reveals that the new events are not systematically more scattered than the original seven. Among the recent events, note in particular Event 11 on 6 August 2001, whose moment (1.44×10^{26} dyn cm) makes it the largest solution published in the CMT Harvard catalog, not only on the Eltanin system, but along the whole Pacific–Antarctic and Pacific–Nazca plate boundaries. The total seismic moment released by the 14 events amounts to 1/5 of the moment released from all strike-slip earthquakes for the relevant period (1977–2001) on the TF systems ranging from (and including) the Menard to Udintsev TFs. The average orientation of the tension axes of the 14 events is N(349 ± 20)°E, i.e., 52° away from the azimuth of the Eltanin TF. Finally, and as discussed by Okal and Langenhorst [4], the occurrence of tensional earthquakes on the Eltanin system is unique, not only along the East Pacific Rise, but also on the Romanche TF

Table 1
Non-strike-slip focal solutions on the Eltanin and adjacent TFs

Number	Date	Epicenter			Transform fault	M_0	Focal solution			Tensional axis	
	D M (J) Y	(°N)	(°E)	Ref.		(10^{24} dyn cm)	ϕ (°)	δ (°)	λ (°)	Plunge (°)	Azimuth (°)
Okal and Langenhorst (2000)											
1	17 FEB (048) 1978	−55.43	−125.14	EHB	Heezen	2.3	256	34	−73	12	154
2	17 SEP (260) 1982	−54.52	−136.65	EHB	Hollister	0.67	59	39	−130	12	357
3	10 OCT (283) 1982	−54.65	−130.55	EHB	Tharp	0.62	97	41	−65	7	349
4	16 AUG (229) 1984	−55.34	−123.72	EHB	Heezen	1.6	81	27	−86	18	348
5	15 MAY (135) 1987	−49.84	−115.29	EHB	Menard	2.1	53	37	−100	8	330
6	27 MAY (147) 1989	−54.76	−132.59	EHB	Tharp	15	72	33	−95	12	346
7	23 AUG (235) 1995	−56.76	−141.39	EHB	Udintsev	27	28	38	−133	14	328
New solutions											
8	1 JUN (152) 1999	−55.59	−123.92	EHB	Heezen	1.08	273	19	−90	26	183
9	4 OCT (278) 2000	−55.49	−128.12	ISC	Tharp	6	257	49	−93	4	349
10	23 JAN (023) 2001	−54.69	−133.33	ISC	Tharp	2.8	300	57	−57	6	7
11	6 AUG (218) 2001	−55.54	−123.42	PDE	Heezen	144	274	46	−97	1	9
12	10 AUG (222) 2001	−55.53	−123.68	PDE	Heezen	0.85	269	58	−101	12	7
13	10 SEP (253) 2001	−56.58	−141.89	PDE	Udintsev	0.45	232	45	−90	0	142
14	12 NOV (316) 2001	−49.59	−116.19	PDE	Menard	4.7	243	51	−114	3	350
Average mechanism											
Unweighted							260	50	−87	5	348
Weighted by moment							267	49	−94	4	360

in the equatorial Atlantic, which features a comparable length of total offset.

A number of suggestions have been made for the origin of the extensional earthquakes observed on the Eltanin TF system. Wolfe et al. [6] proposed that they were related to pull-apart basins located within the TF, and suggested that the changes in fault geometry could be caused by a variety of processes including changes in plate motion, diapiric rise of altered blocks of lower crustal or upper mantle material, volcanic construction, fault normal compression or extension, variability in crustal accretion at adjoining ridge segments, and small deviations of transform strike from the ideal small circle. However, Lonsdale [1] noted that these extensional earthquakes were too large ($m_b = 5.3$–5.5; the subsequent Event 11 being even larger) to be generated at pull-apart basins where the crust is typically thin and hot and may be accreting. Instead, he proposed that the extensional earthquakes along the Heezen and Tharp TFs are caused either indirectly or directly by inside-corner rifting. Such processes are documented at ridge–transform intersections (RTIs) [1], where they have been proposed to explain normal faulting earthquakes [9], and this interpretation could certainly apply to Event 2 on the Hollister TF, Event 14 on the Menard TF, and possibly Event 9 at the eastern end of the Tharp TF (Fig. 1). It would, however, be difficult to

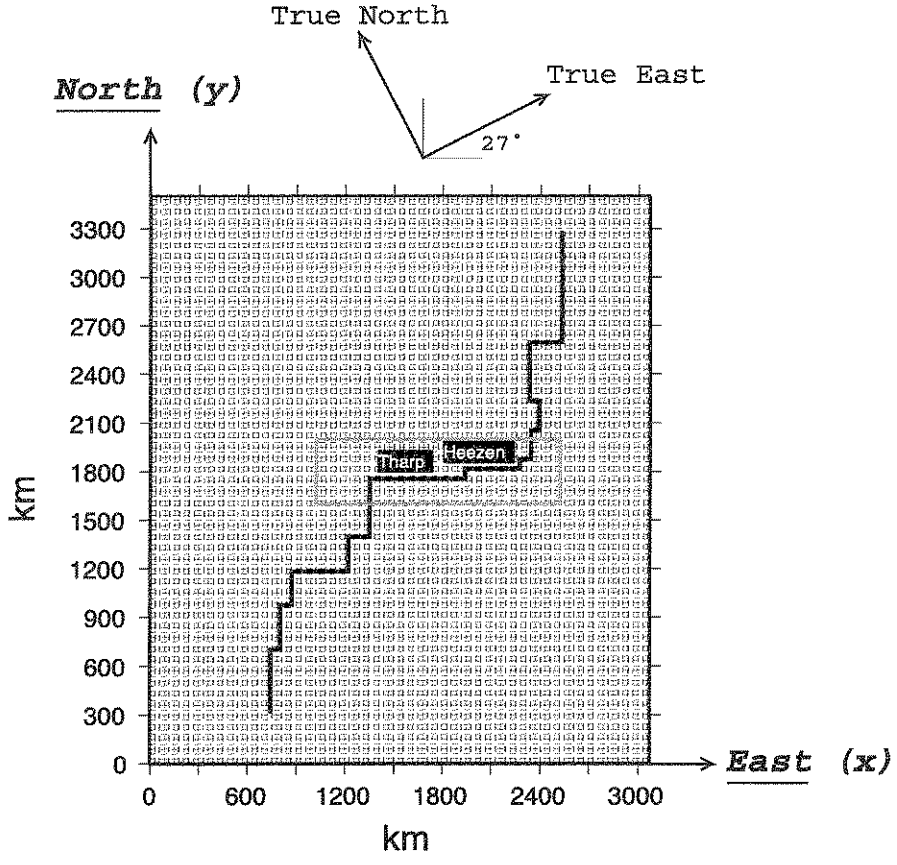

Fig. 2. Finite element grid used for all simulations. The thick trace is the Pacific–Antarctic plate boundary. While the computation is always carried out over the whole grid, Fig. 4 presents only close-ups of the results in the area of the Eltanin TF system, as delimited by the gray box. The axes identify the *north* (y) and *east* (x) directions, rotated 27° clockwise from their true geographic counterparts, as illustrated by the top sketch. The forces and material properties used in the models are listed in the text.

reconcile with the location of the other anomalous events, which cluster at or near the center of the Menard, Udintsev and Heezen TFs, or constitute 'outliers', transversally offset from the TF segment [4].

Wilcock et al. [10] have proposed other possible scenarios for the origin of normal faulting events along the Kane transform in the Central Atlantic. These include differential subsidence under cooling plates bordering the transform, a recent or ongoing change in the location of the spreading pole, and changes in asthenospheric flow. Such mechanisms are most applicable where tension axes are perpendicular to the transform, as observed at the Kane TF. This is not the case on the Eltanin system where the T axes are oriented at an oblique angle to the strike of the TF. A similar geometry for extensional earthquakes has been noted at RTIs and is believed to result from the change in the maximum stress field from ridge-parallel to transform-parallel [11–13].

In this general framework, the present paper explores numerically various models of plate stresses, and seeks to explain the genesis of extensional earthquakes along the Eltanin transform system.

2. Methodology

Our approach in this project is to test the viability of mechanisms proposed for the anomalous earthquakes along the Eltanin transform through numerical computations of various models of the stress field inside a system of plates simulating the geometry of the Eltanin transform system. We use the *FElt* finite element algorithm of Gobat and Atkinson [14], with a variety of boundary conditions, initial conditions (i.e., forces applied to the system), and material properties (i.e., strength of various elements).

Because the Eltanin TF is oriented E27°S (N117°E), and in order to simplify the language, we consider here a coordinate system rotated clockwise 27° from geographic coordinates. In this reference frame, the coordinate directed along the transform (x in the finite element code), will henceforth be referred to as *east*, and the direction (y) across the transform as *north*, always using underlined bold italics for the rotated system, and reserving roman type for the true geographic directions. Thus, in the new coordinate system, the tension axes of the anomalous earthquakes are oriented $N(322 \pm 20)^{\circ}E$ or, essentially, $NW - SE$.

As shown on Fig. 2, we use a 3100 km×3500 km grid, composed mostly of planar, quadrilateral elements of 30 km side, except at the ridges and transforms, where elements are specially aligned, sized and shaped to represent the width and trend of these features. In particular, and as shown on Fig. 3, the width of the TF is taken as 2 km, which is representative of the bottom of the transform troughs [15]. In all our models, we consider two media, a strong one modeling the passive cooled oceanic lithosphere, and a weak one mod-

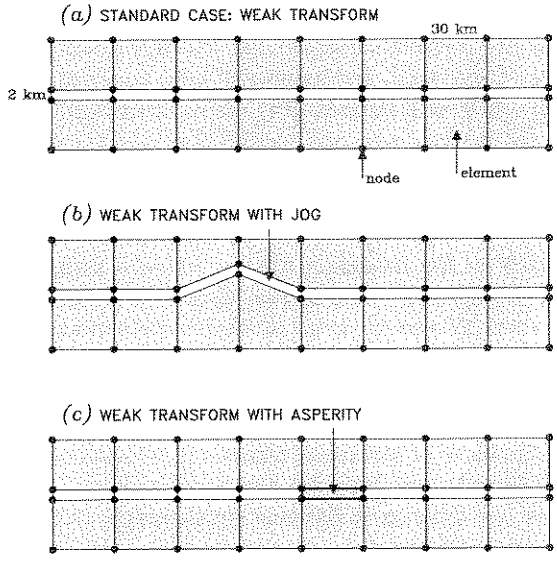

Fig. 3. Close-up showing the finer grid used in the vicinity of a TF segment. In all three diagrams, the shaded areas represent strong elements, while the open ones represent weak elements. For clarity, the TF width (2 km) is not drawn to scale. In (a), we show the model of a standard weak TF, whose results are given on Fig. 4a. In (b), we show the geometry of one of the three identical jogs introduced in the model of Fig. 4b; again, the amplitude of the jog (5 km) is not drawn to scale. In (c), we introduce an asperity defined as a single strong element on an otherwise weak TF, with the resulting stress field given in Fig. 4g. For clarity, the asperity is outlined as a thick contour, but its properties are similar to those of the surrounding lithosphere.

eling the warm active ridges. As discussed below, elements along the transform segments can be taken either as 'strong', having the same material properties as the surrounding lithosphere, or 'weak', having the same material properties as the ridge segments.

Our goal in the present study is to investigate primarily the geometry of the stresses generated in the relevant plates and in particular near their boundaries, under various geometries and different conditions of loading. We emphasize that *FElt* solves the static deformation of a linear elastic system, and that as such, the solution, i.e., the stress field on the grid, is a linear function of the input. Furthermore, it is easily shown that the magnitude of the displacement field will scale as the ratio of the loading to the elastic moduli, and that in turn, the stress field will scale simply with the loading. In other words, and as long as the geometry of the system, the Poisson ratios, and the relative values of the Young's moduli in strong and weak regions are all kept constant, the stress field will depend only on the forces applied to the system, and not on the absolute values of the elastic constants of the materials. Furthermore, the stresses will scale linearly with such forces. In this respect, the critical parameters involved in the modeling are the Poisson ratios of the strong and weak media, which we both take as $\nu = 0.25$, and the ratio of the Young's moduli E for strong and weak media, which we take as 1000 to express the strong decoupling expected at the ridges; Richardson et al. [16] have shown that the distribution of intraplate stresses in oceanic plates is affected very little by the exact value of this ratio, as long as it remains much larger than 1. Further aspects of the implementation of the *FElt* code are detailed in Beutel [17].

All models are then subjected to a system of forces generally referred to as 'ridge push', and expressing gravitational sliding under aging, distributed in the entire interior of the plate as discussed, e.g., by Lister [18] and summarized by Turcotte and Schubert [19]. The actual state of stress of the real-Earth Pacific plate is of course controlled by a more complex combination of forces, including slab pull and collision forces located at the subduction zones (e.g., [20]). However, in the present two-dimensional model, the lack of the third dimension combined with the large distance of the area under study from the locus of the subduction processes, suggest the omission of slab pull and other subduction-related forces as boundary conditions. Rather, and in keeping with the specifications of *FElt*, which require that at least one node be fixed in space, we impose rigid boundary conditions on all edges of the grid, while all nodes and elements within the grid are free to move in any direction. In practice, the boundaries of the model are sufficiently removed from the features under study (i.e., the Eltanin system), so as not to affect the nature of stresses in the vicinity of the latter.

Several authors, including Forsyth and Uyeda [20], have used a simplified representation of ridge push in which it is applied exclusively along the ridge boundary. This approximation is legitimate since ridge push is expected to be strongest at the ridge, where bathymetric gradients are themselves greatest. In addition, it accurately predicts the compressional state of the plate [21]. Here, we elect as a model a variable ridge push force, applied to all nodes in the interior of the plate (except within two nodes of the lateral boundaries of the model). The force is oriented $\underline{E-W}$ and its amplitude varies linearly with the elevation of the seafloor (and thus with $1/\sqrt{\text{age}}$ [22,23], which we model in increments of 10 Ma). Note that the ridge, shown as the $\underline{N-S}$ segments of the thick trace on Fig. 2, is artificially stopped 200 km from the *northern* and *southern* boundaries of the grid to avoid additional edge effects.

As the purpose of the present study is to investigate the nature and orientation of stresses generated under various conditions of loading, and given the linearity of the model, the absolute magnitude of the forces applied on the ridge is largely irrelevant; in this respect, we follow the approach of Forsyth and Uyeda [20], who did not specify an absolute value of the various forces involved in their landmark analysis.

We now describe the family of models used in our investigations, which illustrate several possible tectonic scenarios at the Eltanin TF.

1. We first vary the strength of the TF itself, by considering both 'weak Eltanin' and 'strong

Eltanin' classes of models. In the former, the transform segments share the mechanical properties of the ridge, while in the latter, they share those of the interior of the lithospheric plates. Fig. 3a illustrates the case of a 'weak' TF setting.

2. In the simplest classes of models, we apply ridge push forces perpendicular to the ridge segments, i.e., in an *E – W* direction. We then consider the possibility of a Pliocene change in absolute motion of the Pacific plate [24], in which case we apply ridge push forces rotated 10° clockwise on the Pacific side (in the *N* 80° *W* direction), but keep an *E – W* force on the Antarctic side of the model. This assumes that the Pacific plate changed its motion while the Antarctic plate did not, as discussed in detail by Okal and Langenhorst [4,25]. It also assumes that ridge push will reorient together with the spreading direction, which may be true at the ridge (where the force is expected to be largest), but not in the interior of the plate, where its direction would remain that of the local age gradient, hence of spreading at the time of formation of the lithospheric material. As a worst-case scenario, we rotate the whole force system, and since the latter now features a *northern* component, we refer to this class of models as 10° *N* models.

For completeness, we also investigate the case of a 10° counter-clockwise rotation of the force applied on the Pacific lithosphere, while retaining *eastward* forces on the Antarctic plate, and refer to such models as 10° *S* models.

3. An additional class of models is obtained by allowing small irregularities in the geometry of the transform. The presence of such bends or 'jogs' on fault surfaces is well documented at all scales [26], and their perturbation of the local stress field has been examined by a number of authors (e.g., [27–30]). As illustrated on Fig. 3b, we model the jogs by displacing a single set of nodes a distance of 5 km, perpendicular to the TF. We position the center of the jogs at abscissæ 440 and 760 km on the Tharp TF, and 1080 km on the Heezen TF. The first jog is displaced to the *north*, the other two to the *south*.
4. Finally, we examine the case of the possible existence of strength 'asperities', defined as single elements featuring strong (lithosphere-like) mechanical properties along otherwise weak (ridge-like) TF segments (see Fig. 3c). The concept of fault asperities has its foundation in rock mechanics, where it was recognized that the contact between planar surfaces is highly heterogeneous and in practice concentrated at a discrete number of 'hard spots' or 'asperities'

→

Fig. 4. (a): Results of the finite element modeling in the case of weak TFs. The individual bar symbols represent the orientation of the eigenvectors of the two-dimensional stress field. Open bars are for negative eigenvalues (compressional stress), solid ones for positive eigenvalues (tensional stress); the dimensions of the bars are proportional to the principal stresses. The background shading expresses the sign of the eigenvalue of greatest absolute value, from purple and blue (negative; highly compressional) through green (null) to yellow and red (positive; highly tensional). In this particular case, note the dominant compressional stresses in the central parts of the TF segments. The plate boundary is superimposed in red. (b): Same as (a), with three localized bends introduced on the Tharp TF at abscissæ 440 and 760 km, and on the Heezen TF at 1080 km. Note that the only disruptions in the stress field consist in localized *E – W* compressional stress regimes along the TFs, which are incompatible with the mechanisms on Fig. 1. (c): Same as (a), for the 10° *N* model, in which the ridge push force is applied to the Pacific plate in the *N*80° *W* direction, the transform segments remaining weak. Note the development of a zone of tensional stress expanding into the Pacific plate at the *western* RTI. The state of stress along the TF segments remains essentially unchanged. (d): Same as (c), for the 10° *S* model, in which the ridge push force is applied to the Pacific plate in the *S*80° *W* direction, the TF segments remaining weak. Note this time an increased compression created at the Tharp RTI, but still essentially no change along the TF segments. (e): Same as (a), for the case of a strong Eltanin system, featuring the same mechanical properties as the surrounding lithosphere. Note the development of large zones of tension *inside* the plates in the prolongation of the ridge segments, the latter now being the only weak lines in the grid. (f): Same as (e), for the 10° *N* model, in which the ridge push force is applied to the Pacific plate in the *N*80° *W* direction, the TF segments remaining strong. (g): Same as (a), with asperities located at abscissæ 440 and 760 km on the Tharp TF, and 1080 km on the Heezen TF. Note the concentration of strong tensional stress fields in their immediate vicinity, both on the TF segment and, significantly, inside the plates. (h): Same as (g), with ridge push now oriented *W*10° *N*. Note that the stress field is essentially unchanged from that on (g).

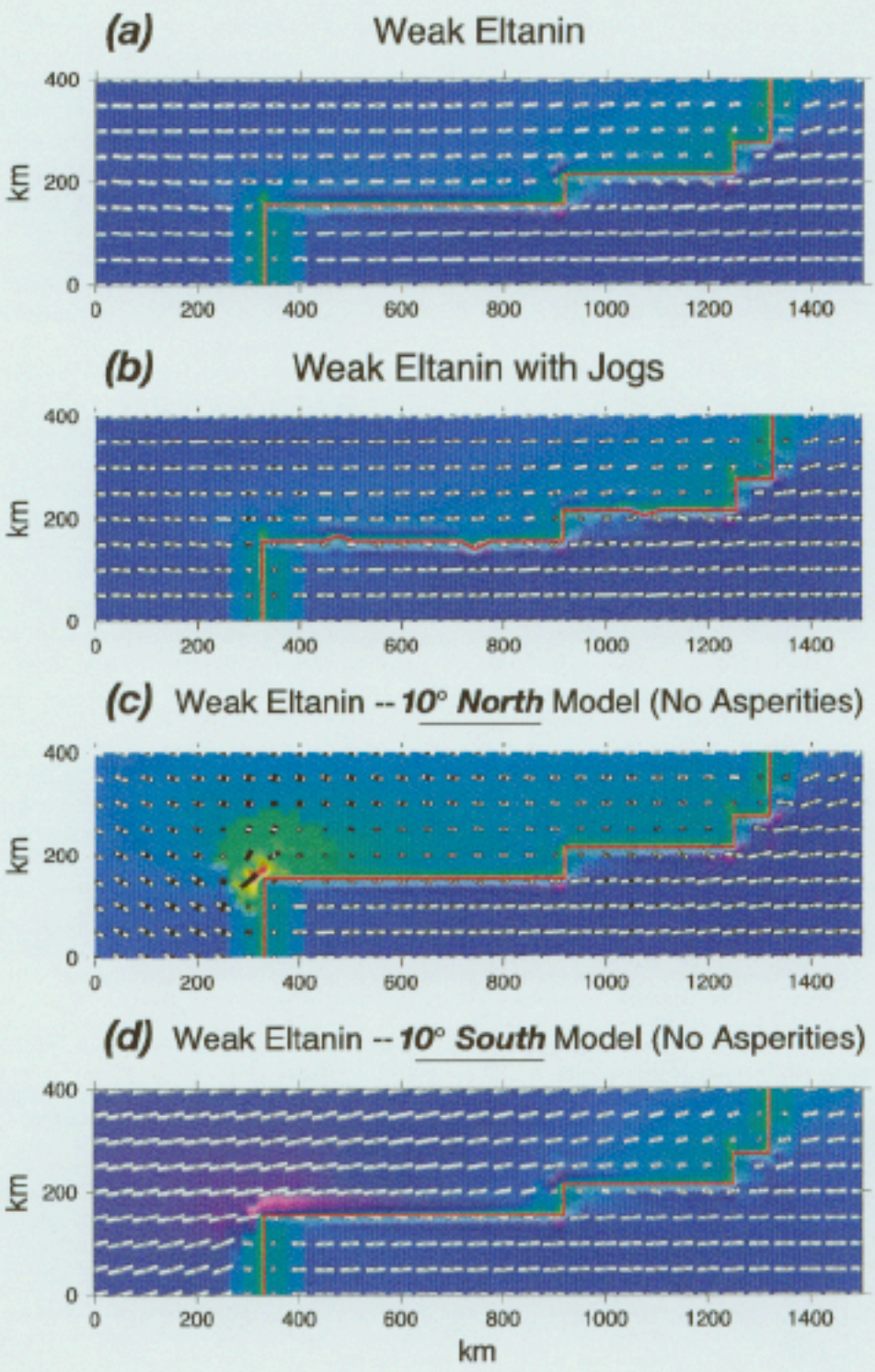
(a) Weak Eltanin
(b) Weak Eltanin with Jogs
(c) Weak Eltanin -- 10° North Model (No Asperities)
(d) Weak Eltanin -- 10° South Model (No Asperities)
km
0
200
400
600
800
1000
1200
1400

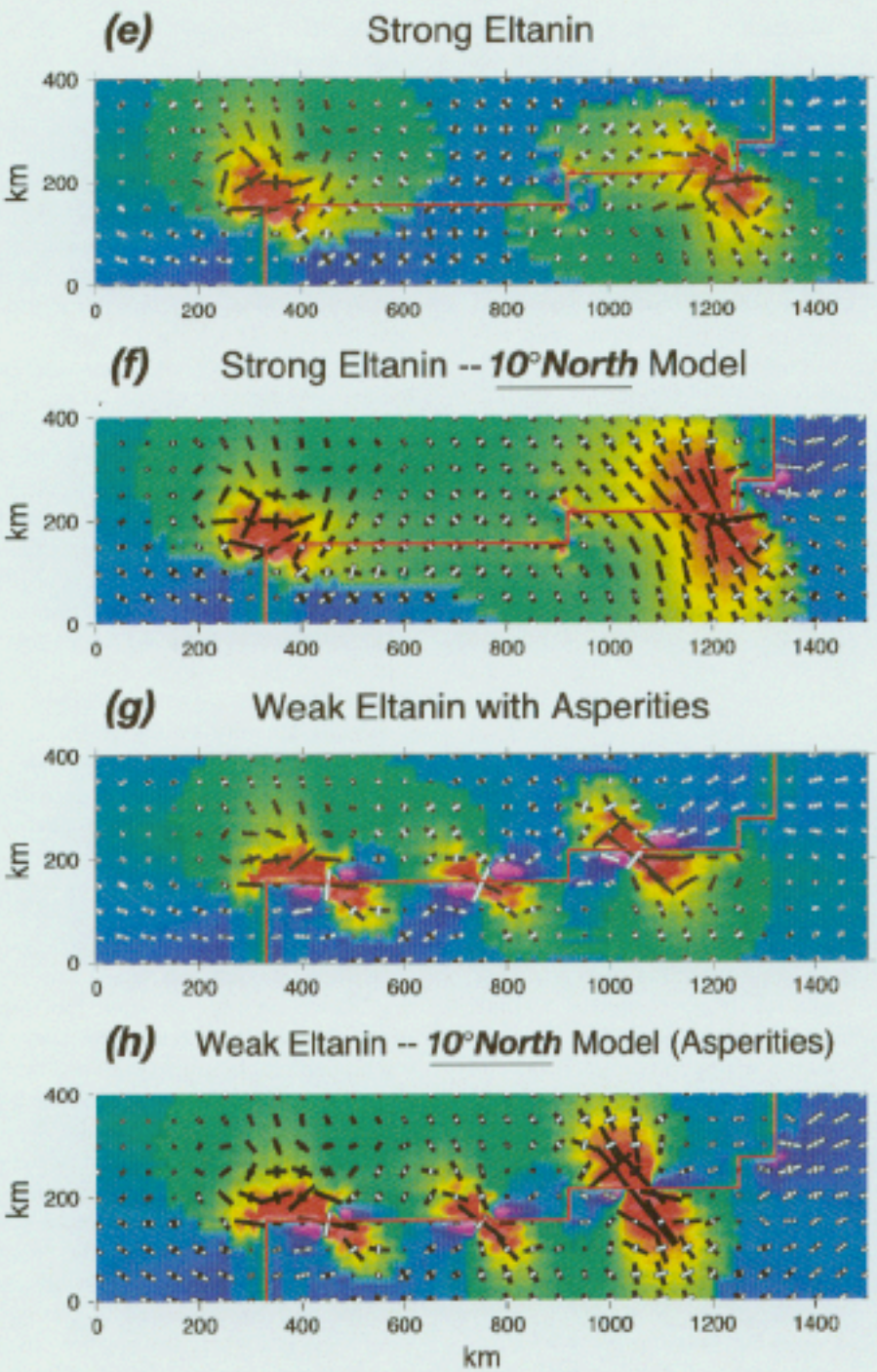

Fig. 4 (*Continued*).

[31]. It was successfully applied to seismic source studies, where it provided a natural explanation to the observed variation of coupling, for example at subduction zones [32,33]. In the case of TFs, the extensive occurrence of hydrothermalism, leading to alteration and metamorphism, as well as the lateral variation of the morphological expression of the TF [6,15] naturally suggest a wide variation in the nature of the contact between the two walls, both amongst TF populations, and laterally within a single TF segment (e.g., [34]), and consequently in the regime of seismic strain release [35].

Selected combinations of the above models (1, 2, 3, 4) are presented in the next section. Fewer variations are presented for the strong TF family of models, on account of both the consistency of the results, and their predominantly irrelevant character when applied to the real-life Eltanin system.

3. Results

Fig. 4 presents the stress fields generated in the vicinity of the Eltanin system for models resulting from various combinations of the parameters described in the previous section. In the absence of a third dimension, we characterize the stress σ_{xy} through its principal elements. The bar symbols give the orientation and amplitude of the eigenstresses (open: negative [compressional]; solid: positive [tensional]). The background is colored according to the nature of the maximum absolute value of principal stress (the eigenvalue of largest amplitude), from purple (compressional) through green (neutral) to red (tensional). Thus, a purple region should always show a prominent open bar, and a red one, a prominent solid bar.

3.1. Weak Eltanin (Fig. 4a–d)

On Fig. 4a, we consider the simple model of a weak Eltanin TF system (i.e., with a strength similar to that of the ridge, but three orders of magnitude lower than for the surrounding lithosphere), with simple $\underline{E-W}$ 'ridge push'. The whole area surrounding the Eltanin system is under essentially uniaxial $\underline{E-W}$ compression. The transform segments themselves are subject to a compressional dominant stress trending $\underline{N60^\circ W}$ with extensional (but low) minimum stress. The ridges remain under very low absolute stress.

In the next model (Fig. 4b), we introduce localized bends in the TF segments (at abscissæ 440 and 760 km along the Tharp TF and 1080 km on the Heezen TF). These result in a localized $\underline{NE-SW}$ trending compressional stress at the bends, but the rest of the model remains essentially unchanged.

We next investigate the case of the $\underline{10^\circ N}$ model, the Eltanin system remaining weak. Fig. 4c shows that the main changes in the stress field are the development of an area under extensional stress at the *western* end of the Tharp TF, and a decrease in the magnitude of the minimum compressional stresses *west* of the transform. The nature and direction of the stress along the Heezen and Tharp TF segments are virtually unchanged.

Results are very similar in the opposite case of the $\underline{10^\circ S}$ model (Fig. 4d), but the RTI at the *western* of the Tharp TF becomes compressional; once again, the transform segments are essentially unaffected.

3.2. Strong transforms

In these models, all transform segments have the same strength as the lithosphere around them; they are only delineated from the surrounding lithosphere by the shape, size and locations of their elements. We first consider a model with ridge push applied in the regular $\underline{E-W}$ direction (Fig. 4e). The principal feature of the stress field is now the development of large zones of tensional stress near the RTIs. This expresses the abrupt termination of the weak ridge segment at the RTI, where it is surrounded on all sides by strong material, as demonstrated at the *western* end of the Tharp TF, where the *northern* plate (Pacific) is under strong tension, while the *southern* segments (both on the Pacific and Antarctic plates) are under minimal stresses. The situation is more complex at the *eastern* end of the Heezen TF seg-

ment; due to the presence of the small TF $5\frac{1}{2}$ offset, the magnitude of the tensional stresses is far greater than in the surrounding lithosphere. Along the long Tharp transform segment, stresses remain of very low amplitude, with comparable compressional and tensional components, oriented $N45°W$, and $N45°E$ respectively.

We have verified that the addition of bends along the TF segments does not affect the stress field in any appreciable way, which was to be expected, since it does not change the overall mechanical properties across the transforms. On the other hand, Fig. 4f shows that reorienting ridge push along $W80°N$ (in a so-called $10°N$ model) results essentially in a slight reduction of the tensional area around the Tharp ridge tip, and in an increase of its counterpart at the Heezen RTI (the reason for the disparity being the greater fragmentation of the Heezen system involving TF $5\frac{1}{2}$).

3.3. Weak Eltanin with strong asperities

We now consider a model in which we embed three small strong areas in the otherwise weak transform segments, to simulate a locally locked TF. These asperities are placed at abscissæ 440, 760 km (on the Tharp TF), and 1080 km (on the Heezen TF), i.e., at the approximate location of the observed anomalous earthquakes. As shown on Fig. 3c, they each consist of a single strong element, 30 km long and 2 km wide.

Fig. 4g shows that the asperities, rather than the RTIs, now dominate the stress field. Each asperity gives rise to a local stress concentration featuring compression in the $NE-SW$ direction and extension in the $NW-SE$ one. These fields dominate not only the asperities and the immediate area, but the lithosphere around the transform segments as well; this pattern constitutes a major change in the overall stress field of the TFs when compared with the previous models of the state of stress. In the example chosen, the tensional stress field at the exact location of the *westernmost* asperity nearly parallels the TF; however the stress field is so heterogeneous in this area that the nearby grid points, especially outside the TF segment, are more representative of the local state of stress.

Further combining the presence of asperities with reoriented ridge push (e.g., in the $W10°N$ direction; Fig. 4h) results in only insignificant changes in the properties of the stress field, which remains dominated by the asperities.

4. Discussion

In this section, we compare the results obtained numerically from our various models to the observed characteristics of the seismicity occurring along the Eltanin system. Any successful model of the mechanical properties of the system must explain both the substantial deficiency in seismic moment release and the occurrence of normal faulting events with a T axis oriented $NW-SE$. We conclude that the Eltanin system is best modeled as weak TFs featuring local asperities.

At first order, one would expect plate motions to parallel the TF system, and TF segments to feature largely homogeneous strength in a direction parallel to their strike, with any variations in strength occurring on a scale less rapid than those in thermal state, controlled by the age gradients on the two plates. Both homogeneous models studied, namely the simple 'weak Eltanin' and 'strong Eltanin' cases (Fig. 4a and e, respectively), result in weak $NW-SE$ compression across the TF segments, inclined at a lesser angle (35°) on a weak TF than on a strong one (45°), as predicted by Hatcher [36]. This agreement can be regarded as an a posteriori confirmation of the validity of our computational models.

We believe that the Eltanin TF system is best modeled as weak, on two accounts: first, its 90% deficiency in seismic moment release when compared to kinematic models [3,4] implies minimal coupling along the TF segments; and second, the absence of compelling evidence for the concentration of stress at the tips of the spreading segments, near the RTIs, which would be predicted by our strong Eltanin modeling. This result is in agreement with the generally weak character of major faults, as proposed by Hubbert and Rubey [37], and reported, e.g., by Zoback et al. [38] in the case of the San Andreas system.

In general, weak mechanical properties along TFs have been interpreted as resulting from pro-

cesses of fracturing, hydrothermal alteration, and metamorphism, which have been widely documented in many TF segments of the mid-oceanic ridge system (e.g., [39–42]). Along the ultra-fast Garrett TF, Hekinian et al. [43] have even documented pockets of volcanic activity within the transform segment, which are not directly associated with any identifiable offset. Along the Eltanin system itself, Lonsdale [15] has suggested that seismic deficiency could be explained by an anomalously thin crust (perhaps not exceeding 1 km), together with the pervasive serpentinization of sub-crustal rocks.

Having thus eliminated the 'strong' models, and in order to explain the origin of the tensional earthquakes, we discuss the three possible modifications of the background model of a weak Eltanin transform, namely oblique ridge push on the Pacific plate, bends or asperities along the TF segments.

Changes in ridge push orientation were motivated by Wessel and Kroenke's suggestion of a Pliocene change in the absolute motion of the Pacific plate over the mantle [24]. However, we find that the application of a $N-S$ component to the ridge push (either *northward* in the $10°N$ model or *southward* in the $10°S$ one) induces significant changes only in regions close to the RTIs, and not along the TF segments. As such, these models cannot explain the location of the anomalous earthquakes, as mapped on Fig. 1.

Similarly, we find that the introduction of bends ('jogs') in the geometry of TF segments (without changes in strengths) modifies only nominally the stress field along the segments, and cannot explain the presence of tensional earthquakes in their center.

By contrast, the introduction of strong asperities clearly brings heterogeneity to the stress field along the TF segments. The corresponding models correctly predict the development of large regions of $NW-SE$ tensional stress, centered at the asperities and extending away from them in a $NW-SE$ direction. Our models explain both the orientation of the T axes of the relevant earthquakes (essentially $N45°W$) and the fact that they can occur both on the TF segments and as outliers to the precise plate boundary defined by the background seismicity (e.g., Events 6, 10), as discussed by Okal and Langenhorst [4].

If indeed asperities are present locally along an otherwise weak Eltanin TF system, one might expect enhanced strike-slip activity at their location. To explore this possibility, we plot as open triangles on Fig. 1 the nine largest strike-slip CMT solutions in the study area ($M_0 = 3.0–5.3 \times 10^{25}$ dyn cm). The results are mixed, and must be regarded as inconclusive: while on the Udintsev and Hollister TFs, large strike-slip events do take place in the vicinity of tensional earthquakes, this is not the case on the Heezen and Menard TFs, where the former congregate preferentially at the *eastern* RTIs; also, none of the nine largest strike-slip events are found on the Tharp TF. At any rate, the apparent correlation found on the Udintsev and Hollister TFs should not be overinterpreted; in particular, we stress the small size of even the largest strike-slip solution in the CMT catalog ($M_0 = 5.3 \times 10^{25}$ dyn cm). Furthermore we have no insight into the true size of any possible asperity, which we have chosen to model as a single element of our grid (30 km), only for convenience; any smaller asperity could only entertain an even smaller strike-slip earthquake.

Having established that the release of tensional stress on and in the vicinity of the TF segments of the Eltanin system can be adequately explained by the presence of strong asperities on an otherwise weak fault, we present some ideas and speculations as to their possible origin. We seek to explain why such asperities would develop on the TFs of the Eltanin system, but be absent from other large transforms along the mid-oceanic ridges.

It is difficult to argue in favor of purely geometric and kinematic factors playing a role in the development of asperities. While the length of the Eltanin offset is unparalleled in the South Pacific, it is actually split into two segments, the longest one (the Tharp TF) not exceeding 480 km. The half-spreading rate of 4.2 cm/yr results in a maximum age of 11 Ma for the material in contact along the Tharp TF. This number is neither large nor small, being rather typical of the age of ocean floor along shorter but slower TF segments of the MOR system; in other words, the geometric pa-

rameters of the Eltanin system do not in themselves provide for the juxtaposition of material with thermally induced large disparities, and do not provide a framework to suggest a different regime of contact. Furthermore, tensional earthquakes are also documented in the central sections of the much shorter Udintsev and Menard TFs.

Rather, we think that the presence of strong asperities along the walls of the Eltanin TFs may be related to their disturbed morphology, as described by Lonsdale [15], itself a probable result of the complex history of spreading in the South Pacific, first investigated by Molnar et al. [44]. According to these authors' reconstructions, the Eltanin system formed as a prominent offset as early as the Upper Eocene, but underwent changes in orientation and spreading rates, possibly associated with an episode of large-scale ridge propagation south of the Udintsev system [45,46], and involving reorientation as recent as the Pliocene [47]. The detailed mapping by Lonsdale [1] suggests that the transform valley can be occasionally filled by volcanic structures, which, he proposes, express local spreading. We speculate that should such features become inactive, they may conceivably develop into asperities, after they have equilibrated thermally from an originally hotter state, and as the excess volume in their morphology becomes an obstacle to smooth strike-slip motion.

Finally, we note that our stress model, as presented on Fig. 4g, would also suggest the possible release of compressional stress in the opposite quadrants surrounding the asperities, i.e., to the *NE* and *SW* of their locations on the TF segments. The absence of compressional earthquakes on the Eltanin system may reflect the lower strength of lithospheric rocks when loaded under tension as opposed to compression (e.g., [48]).

5. Conclusions

Two-dimensional finite element models suggest that the anomalous normal faulting earthquakes with T axes trending N10°W, observed along the Eltanin transform system and its immediate neighbors (Udintsev, Menard), are the product of a generally weak TF (as also indicated by the significant deficiency in seismic moment release) and the presence of strong asperities. The latter, when embedded in an otherwise weak TF, create an inhomogeneous stress field where the greatest stresses are no longer located near the RTIs, as in the unperturbed model, but in the vicinity of the asperities, both on the TF segment, and in the nearby plate interiors. These localized stress fields feature eigendirections oriented *NE – SW* (i.e., N72°E) for the compressional axis, and *NW – SE* (i.e., N18°W) for the tensional one, the latter in excellent agreement with the observed focal mechanisms (on the average N11°W ± 20°). Thus, the asperity model can explain both the location and the focal geometry of the anomalous earthquakes. We speculate that the development of asperities along the Eltanin transforms and their neighbors may be traced to the complex history of readjustments in the direction and rate of spreading of the southern part of the Pacific–Antarctic plate boundary, resulting in the observed perturbation of the morphology of the transform valley and of its walls, as documented from the small-scale bathymetric surveys of Lonsdale [1,15].

Acknowledgements

We are grateful to Craig Bina for discussion and to Bob Engdahl for providing his latest relocated catalog, updated from [8]. The paper benefited from constructive reviews from Randy Richardson, John Sclater, and an anonymous reviewer. Most figures were drafted using the GMT software [49]. *[SK]*

References

[1] P. Lonsdale, Structural geomorphology of the Eltanin fault system and adjacent transform faults of the Pacific–Antarctic plate boundary, Mar. Geophys. Res. 16 (1994) 105–143.
[2] C. DeMets, R.G. Gordon, D.F. Argus, S. Stein, Current plate motions, Geophys. J. Int. 101 (1990) 425–478.
[3] L.M. Stewart, E.A. Okal, Seismicity and aseismic slip

along the Eltanin Fracture Zone, J. Geophys. Res. 88 (1983) 10495–10507.
[4] E.A. Okal, A.R. Langenhorst, Seismic properties of the Eltanin Transform System, South Pacific, Phys. Earth Planet. Inter. 119 (2000) 185–208.
[5] M.E. Wysession, E.A. Okal, K.L. Miller, Intraplate seismicity of the Pacific Basin, 1913–1988, Pure Appl. Geophys. 135 (1991) 261–359.
[6] C.J. Wolfe, E.A. Bergman, S.C. Solomon, Oceanic transform earthquakes with unusual mechanisms or locations; relation to fault geometry and state of stress in the adjacent lithosphere, J. Geophys. Res. 98 (1993) 16187–16211.
[7] A.M. Dziewonski, G. Ekström, N. Maternovskaya, Centroid-moment tensor solutions for April–June 1999 (and subsequent solutions published on Harvard University's web site), Phys. Earth Planet. Inter. 119 (2000) 161–171.
[8] E.R. Engdahl, R.D. van der Hilst, R.P. Buland, Global teleseismic earthquake relocation with improved travel times and procedures for depth determination, Bull. Seismol. Soc. Am. 88 (1998) 722–743.
[9] J.F. Engeln, Seismological studies of the tectonics of divergent plate boundaries, Ph.D. Dissertation, Northwestern University, Evanston, IL, 1986, 138 pp.
[10] W.S. Wilcock, G.M. Purdy, S.C. Solomon, Microearthquake evidence for extension across the Kane Transform Fault, J. Geophys. Res. 95 (1990) 15439–15462.
[11] J.F. Engeln, D.A. Wiens, S. Stein, Mechanisms and depths of Atlantic transform earthquakes, J. Geophys. Res. 91 (1986) 548–577.
[12] P.Y. Huang, S.C. Solomon, E.A. Bergman, J.L. Nábělek, Focal depths and mechanisms of Mid-Atlantic Ridge earthquakes from body waveform inversion, J. Geophys. Res. 91 (1986) 579–598.
[13] A. Gudmundsson, Stress fields associated with oceanic transform faults, Earth Planet. Sci. Lett. 136 (1995) 603–614.
[14] J. Gobat, D. Atkinson, *FElt*: User's Guide and Reference Manual, University of California, San Diego, CA, 1994, 234 pp.
[15] P. Lonsdale, Tectonic and magmatic ridges in the Eltanin fault system, South Pacific, Mar. Geophys. Res. 8 (1986) 203–242.
[16] R.M. Richardson, S.C. Solomon, N.H. Sleep, Tectonic stress in the plates, Rev. Geophys. Space Phys. 17 (1979) 981–1017.
[17] E.K. Beutel, Relative and absolute plate motion changes in the Southeast Pacific: cause and effect, Ph.D. Dissertation, Northwestern University, Evanston, IL, 2000, 320 pp.
[18] C.R.B. Lister, Gravitational drive on oceanic plates caused by thermal contraction, Nature 257 (1975) 663–665.
[19] D.L. Turcotte, G. Schubert, Geodynamics, Wiley, New York, 1982, 450 pp.
[20] D.W. Forsyth, S. Uyeda, Of the relative importance of the driving forces of plate motion, Geophys. J. R. Astron. Soc. 43 (1975) 163–200.
[21] M.L. Zoback, The World Stress Map Project, J. Geophys. Res. 97 (1992) 11703–12013.
[22] A.M. Tréhu, Depth versus age$^{1/2}$: a perspective on mid-oceanic rises, Earth Planet. Sci. Lett. 27 (1975) 287–304.
[23] C.M.R. Fowler, The Solid Earth, An Introduction to Global Geophysics, Cambridge University Press, Cambridge, 1990, 472 pp.
[24] P. Wessel, L.W. Kroenke, The geometric relationship between hot spots and seamounts; implications for Pacific hot spots, Earth Planet. Sci. Lett. 158 (1998) 1–18.
[25] E.A. Okal, A.R. Langenhorst, Reply [to comment by P. Wessel and L.W. Kroenke], Phys. Earth Planet. Inter. 123 (2001) 81–83.
[26] C.H. Scholz, C.A. Aviles, The fractal geometry of faults and faulting, in: S. Das, J. Boatwright, C.H. Scholz (Eds.), Earthquake Source Mechanics, Am. Geophys. Un. Maurice Ewing Ser. 6, 1986, pp. 147–155.
[27] P. Segall, D.D. Pollard, Mechanics of discontinuous fields, J. Geophys. Res. 85 (1980) 4337–4350.
[28] R.H. Sibson, Rupture interactions with fault jogs, in: S. Das, J. Boatwright, C.H. Scholz (Eds.), Earthquake Source Mechanics, Am. Geophys. Un. Maurice Ewing Ser. 6, 1986, pp. 157–167.
[29] F. Saucier, E. Humphreys, R. Weldon II, Stress near geometrically complex strike-slip faults: Application to the San Andreas Fault at Cajon Pass, Southern California, J. Geophys. Res. 97 (1992) 5081–5094.
[30] M. Dragoni, A. Piombo, Displacement and stress fields around a fault jog; effects on fault mechanics, Phys. Chem. Earth 21 (1996) 237–240.
[31] J.C. Jaeger, N.G.W. Cook, Fundamentals of Rock Mechanics, Wiley, New York, 1976, 585 pp.
[32] J.E. Ebel, Evidence for fault asperities from systematic time-domain modeling of teleseismic waveforms, Ph.D. Dissertation, California Institute Technology, Pasadena, CA, 1981, 149 pp.
[33] T. Lay, H. Kanamori, An asperity model of large earthquake sequences, in: D.W. Simpson, P.G. Richards (Eds.), Earthquake Prediction: An International Review, Am. Geophys. Un. Maurice Ewing Ser. 4, 1981, pp. 79–592.
[34] J.A. Karson, Variations in structure and petrology in the Coastal Complex, Newfoundland; anatomy of an oceanic fracture zone, in: I.G. Gass, S.J. Lippard, A.W. Shelton (Eds.), Ophiolites and Oceanic Lithosphere, Geol. Soc. (London) Spec. Publ. 13, 1984, pp. 131–144.
[35] L.M. Stewart, Strain release along oceanic transform faults, Ph.D. Dissertation, Yale University, New Haven, CT, 1983, 275 pp.
[36] R.D. Hatcher Jr., Structural Geology: Principles, Concepts, and Problems, Merrill Publishing Company, Columbus, OH, 1990, 531 pp.
[37] M.K. Hubbert, W.W. Rubey, Role of pore pressure in the mechanics of overthrust faulting, Geol. Soc. Am. Bull. 70 (1959) 115–166.
[38] M.D. Zoback et al., New evidence on the state of stress of

the San Andreas Fault system, Science 238 (1987) 1105–1111.
[39] E.H. Rutter, K.H. Brodie, On the mechanical properties of oceanic transform faults, Ann. Tectonicæ 1 (1987) 87–96.
[40] M. Cannat, D. Bideau, R. Hébert, Plastic deformation and magmatic impregnation in serpentinized ultramafic rocks from the Garrett Transform fault (East Pacific Rise), Earth Planet. Sci. Lett. 101 (1990) 216–232.
[41] D. Bideau, R. Hébert, R. Hekinian, M. Cannat, Metamorphism of deep-seated rocks from the Garrett ultrafast transform (East Pacific Rise near 13°25′S), J. Geophys. Res. 96 (1991) 10079–10099.
[42] M. Cannat, M. Seyler, Transform tectonics, metamorphic plagioclase and amphibolization in ultramafic rocks of the Vema Transform fault (Atlantic Ocean), Earth Planet. Sci. Lett. 133 (1995) 283–298.
[43] R. Hekinian, D. Bideau, M. Cannat, J. Francheteau, R. Hébert, Volcanic activity and crust-mantle exposure in the ultrafast Garrett Transform Fault near 13°28′S in the Pacific, Earth Planet. Sci. Lett. 108 (1992) 259–275.
[44] P. Molnar, T. Atwater, J. Mammerickx, S.M. Smith, Magnetic anomalies, bathymetry and the tectonic evolution of the South Pacific since the Late Cretaceous, Geophys. J. R. Astron. Soc. 40 (1975) 383–420.
[45] S.C. Cande, C.A. Raymond, J.M. Stock, W.F. Haxby, Geophysics of the Pitman Fracture Zone and Pacific–Antarctic plate motions during the Cenozoic, Science 270 (1995) 947–953.
[46] M. Sahabi, L. Géli, J.-L. Olivet, L. Gilg-Capar, G. Roult, H. Ondréas, P. Beuzart, D. Aslanian, Morphological reorganization within the Pacific–Antarctic discordance, Earth Planet. Sci. Lett. 137 (1996) 157–173.
[47] C.L. Mayes, L.A. Lawver, D.T. Sandwell, Tectonic history and new isochron chart of the South Pacific, J. Geophys. Res. 95 (1990) 8543–8567.
[48] W.F. Brace, D.L. Kohlstedt, Limits on lithospheric stress imposed by laboratory experiments, J. Geophys. Res. 85 (1980) 6248–6252.
[49] P. Wessel, W.H.F. Smith, Free software helps map and display data, EOS Trans. Am. Un. 72 (1991) 441 and 445–446.